Dual-beam ELF wave generation as a function of power, frequency, modulation waveform, and receiver location

D. Agrawal[1] and R. C. Moore[1]

Received 23 June 2012; revised 12 October 2012; accepted 15 October 2012; published 8 December 2012.

[1] Dual-beam ELF wave generation experiments performed at the High-frequency Active Auroral Research Program (HAARP) HF transmitter are used to investigate the dependence of the generated ELF wave magnitude on HF power, HF frequency, modulation waveform, and receiver location. During the experiments, two HF beams transmit simultaneously: one amplitude modulated (AM) HF beam modulates the conductivity of the lower ionosphere at ELF frequencies while a second HF beam broadcasts a continuous waveform (CW) signal, modifying the efficiency of ELF conductivity modulation and thereby the efficiency of ELF wave generation. We report experimental results for different ambient ionospheric conditions, and we interpret the observations in the context of a newly developed dual-beam HF heating model. A comparison between model predictions and experimental observations indicates that the theoretical model includes the essential physics involved in multifrequency HF heating of the lower ionosphere. In addition to the HF transmission parameters mentioned above, the model is used to predict the dependence of ELF wave magnitude on the polarization of the CW beam and on the modulation frequency of the modulated beam. We consider how these effects vary with ambient *D*-region electron density and electron temperature.

Citation: Agrawal, D., and R. C. Moore (2012), Dual-beam ELF wave generation as a function of power, frequency, modulation waveform, and receiver location, *J. Geophys. Res.*, *117*, A12305, doi:10.1029/2012JA018061.

1. Introduction

[2] Extremely low frequency (ELF, 3–3000 Hz) and very low frequency (VLF, 3–30 kHz) waves can be generated by modulated high frequency (HF, 3–30 MHz) heating of the *D*-region ionosphere (~60–100 km altitude) in the presence of naturally forming electric currents, such as the auroral electrojet [e.g., *Getmantsev et al.*, 1974; *Stubbe et al.*, 1982; *Papadopoulos et al.*, 2003; *Moore et al.*, 2007; *Cohen et al.*, 2010]. The magnitude of ELF/VLF waves generated in this manner are dependent upon the ambient ionospheric conditions, such as the electron density and the electron temperature [e.g., *Tomko et al.*, 1980; *Stubbe et al.*, 1982; *Barr and Stubbe*, 1984; *James et al.*, 1984; *Rietveld and Stubbe*, 1987; *Papadopoulos et al.*, 1990; *Barr and Stubbe*, 1991a, 1991b; *Moore*, 2007; *Cohen et al.*, 2010; *Moore and Agrawal*, 2011], as well as on the background geomagnetic conditions that drive the strength of the auroral electrojet [e.g., *Stubbe et al.*, 1981; *Rietveld et al.*, 1983; *Papadopoulos et al.*, 2003; *Payne*, 2007; *Jin et al.*, 2011]. Additionally, in an effort to understand the dynamics of high power radio wave heating of the ionosphere, a number of studies have investigated the dependence of the generated ELF/VLF signal strength on the HF transmission parameters, such as HF power, HF polarization, and modulation frequency [e.g., *Ferraro et al.*, 1984; *Barr and Stubbe*, 1991a, 1991b; *Villaseñor et al.*, 1996; *Milikh et al.*, 1999; *Moore et al.*, 2006; *Fujimaru and Moore*, 2011]. With the completion of hardware upgrades at the High frequency Active Auroral Research Program (HAARP) HF transmitter in Gakona, Alaska in 2007, studies focused on the interactions between two powerful HF radio waves in the ionosphere can now be performed regularly. This paper presents experimental observations performed during one particular type of dual-beam HF heating experiment, focusing on the generation of ELF waves using one amplitude modulated (AM) HF beam and one continuous waveform (CW) HF beam, as depicted schematically in Figure 1.

[3] Recently, *Moore and Agrawal* [2011] critically evaluated the ELF/VLF signal magnitudes generated using one AM beam and one CW beam at HAARP. They compared observations performed during CW-OFF periods and CW-ON periods (with CW power at 100%) for one combination of HF frequencies. Among the various experimental measurements performed, they determined that additional CW heating had the largest impact on the received ELF/VLF signal magnitude, and they suggested that measurable changes in ELF/VLF signal magnitude would result for different combinations of HF frequencies and for different levels of CW power.

[4] In the present paper, we directly evaluate the predictions made by *Moore and Agrawal* [2011], using the same dual-beam HF heating method but employing ten different CW power levels (including CW-OFF) and four distinct HF

[1]Department of Electrical and Computer Engineering, University of Florida, Gainesville, Florida, USA.

Corresponding author: D. Agrawal, Department of Electrical and Computer Engineering, University of Florida, 570 NEB, PO Box 116130, Gainesville, FL 32611, USA. (divya@ufl.edu)

0148-0227/12/2012JA018061

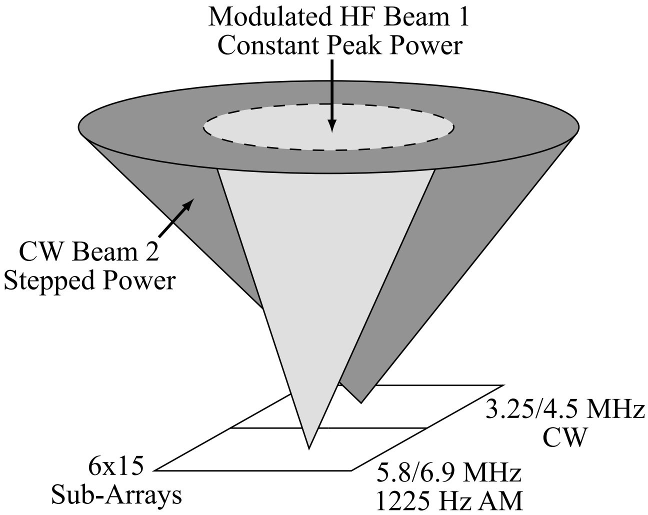

Figure 1. A cartoon diagram of the Dual-Beam HF heating experiment, showing the modulated HF beam (constant peak power) and the power-stepped CW beam. The CW beam is broader than the modulated HF beam.

frequency combinations. Additionally, we perform the experiment using five different modulation waveforms and present observations performed at three significantly different distances from HAARP (3 km, 33 km, and 98 km). The experimental observations are compared to the predictions of a dual-beam ionospheric HF heating model [*Moore and Agrawal*, 2011], demonstrating that the model properly characterizes the ELF wave magnitude dependence on the transmission parameters. The dual-beam HF heating model is further employed to predict the dependence of ELF wave magnitude on the polarization of the CW beam and on the modulation frequency of the modulated HF beam. Within the context of this model, we establish that the ELF signal magnitude is sensitively dependent on the altitude distribution of both the electron density and the electron temperature within the *D*-region ionosphere, and we identify conditions under which the two parameters may be decoupled. Based on the experimental observations and the theoretical calculations presented herein, we suggest that dual-beam HF heating experiments may possibly be used as part of a *D*-region diagnostic in the future.

[5] This paper progresses in the following manner: Section 2 describes the experiment and provides an overview of the instrumentation employed; Section 3 presents a general description of experimental observations performed during the dual-beam HF heating experiment; and Section 4 directly compares the observations and model predictions. Section 5 provides a discussion and a summary of the presented material.

2. Description of the Experiment

[6] The 3.6 MW HAARP HF transmitter located at Gakona, Alaska (62.39°N, 145.2°W) consists of a 12 × 15 array of crossed dipole antennas (360 active elements). During three half-hour periods on 20, 21, and 25 July 2011, HAARP used a dual-beam heating configuration for which the HF array was split into two 6 × 15 (1800 kW) sub-arrays capable of simultaneously transmitting two independent HF beams at different HF frequencies. The first sub-array broadcast an amplitude modulated HF signal in order to generate ELF waves; we will refer to the modulated beam as Beam 1. At the same time, the second sub-array broadcast a CW wave at a different HF frequency and varied the power of the transmission; we will refer to the CW beam as Beam 2. The center frequency for Beam 1 alternated between 5.8 and 6.9 MHz (X-mode), and the peak power was held constant at 100%. The modulation was driven at 1225 Hz using five different modulation waveforms: square, sinusoid, square-root-sinusoid (sqrt-sine), triangle, and sawtooth. The center frequency for Beam 2 alternated between 3.25 and 4.5 MHz (X-mode), resulting in four different HF frequency combinations between Beam 1 and Beam 2. The center frequency of Beam 2 was selected to be lower than that of Beam 1 in order to bathe the entire modulated ionospheric region with CW power, as depicted in the cartoon diagram of Figure 1. The peak power of Beam 2 increased (in 1-dB steps) from −8 dB to 0 dB (full power), resulting in ten CW power levels (including CW-OFF). Each CW power level was held constant for a one-second duration, and the CW transmission alternated between CW-OFF and CW-ON every other second to provide a means to evaluate changes in the electrojet field strength [*Barr and Stubbe*, 1993]. For each frequency combination, the 18-second transmission format was repeated five times: once for each modulation waveform.

[7] Figure 2 maps the locations of the ELF receiver sites relative to HAARP. ELF receivers were located at Oasis (OA, 62.35°N, 145.1°W, 3 km from HAARP), Sinona Creek (SC, 62.58°N, 144.6°W, 33 km from HAARP), and Paradise (PD, 62.52°N, 143.2°W, 98 km from HAARP). Each receiver system consists of two orthogonal magnetic loop antennas oriented to detect the radial and azimuthal components of the magnetic field at ground level, a preamplifier, a line receiver, and a digitizing computer. Accurate timing is provided by a GPS clock. The receiver is sensitive to magnetic fields with frequencies between ~300 Hz and ~45 kHz.

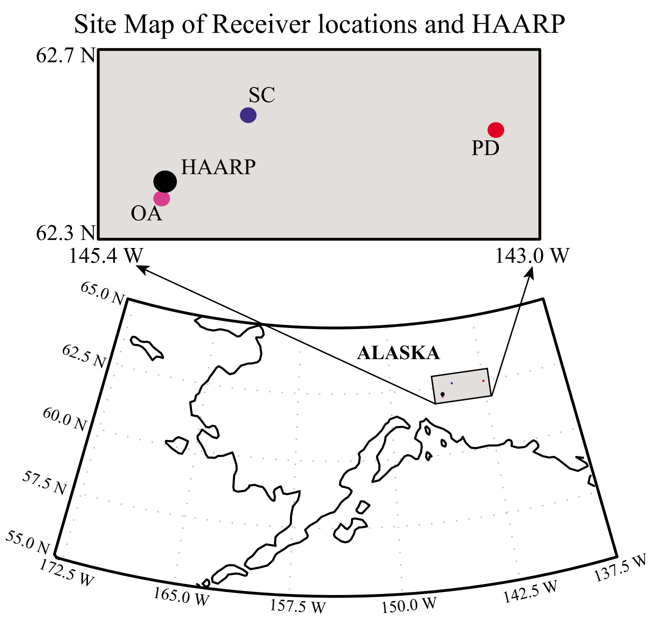

Figure 2. A map of ELF receiver locations relative to HAARP. Oasis (OA), Sinona Creek (SC), and Paradise (PD) are approximately 3, 33, and 98 km from the HAARP facility, respectively.

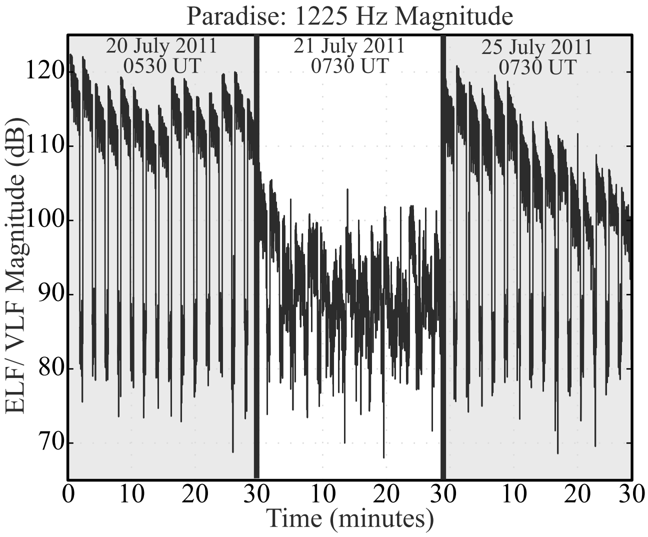

Figure 3. 1225 Hz signal magnitude observed at Paradise (PD) on 20, 21, and 25 July 2011. The highlighted gray backgrounds identify periods of high (>10 dB) SNR.

The signals were sampled at 100 kHz with 16-bit resolution. In post-processing, the amplitudes and phases of the received ELF tones were determined using 1-second-long discrete Fourier transforms.

3. Description of the Data Set

[8] Figure 3 shows the first harmonic ELF signal magnitude (at 1225 Hz) received at Paradise during the three thirty-minute duration transmission blocks on 20, 21, and 25 July 2011. Signals with high (>10 dB) signal-to-noise ratio (SNR) were observed throughout the half-hour transmission periods on 20 July and 25 July. Our analysis will focus on observations performed during these two days, which are highlighted with a gray background in Figure 3. On both days, the HAARP fluxgate magnetometer registered magnetic field fluctuations of over 100 nT during the transmission periods, and the k_p index was 3+. The level of absorption, as measured by the 30-MHz HAARP riometer, was much higher on 20 July (~0.2 dB) than on 25 July (<0.1 dB). Additionally, ionospheric electron density profile estimations performed by the HAARP digisonde at the times of transmission indicate that the ionospheric profiles were dramatically different on the two days, even in the *D*-region: the electron density at 100 km was $\sim 3.6 \times 10^4/\mathrm{cm}^3$ on 20 July, whereas it was less than $1.2 \times 10^4/\mathrm{cm}^3$ on 25 July. The comparison of observations performed on these two days will thus be used to experimentally investigate dual-beam ELF wave generation as a function of ambient ionospheric conditions.

[9] Figure 4 shows 90-second spectrograms of the magnetic field recordings performed at Paradise on 20 July 2011. Figures 4 (top) and 4 (bottom) correspond to the North-South (NS) and East-West (EW) channels of the receiver, respectively. During this 90-second period, HAARP broadcast five 18-second formats, one for each of the five different modulation waveforms employed. In order, these are: square, sinusoid, sqrt-sine, triangle, and saw-tooth waveforms. In all cases, the first harmonic at 1225 Hz is clearly visible in the spectrograms for each channel. Higher-order harmonic content is observed to depend on the modulation waveform. While observations of the higher-order harmonics are important, this paper will focus solely on the first harmonic component.

[10] Figure 5 (bottom) shows the magnitude of the 1225 Hz tones observed at Paradise during the 30 minute transmission period on 20 July 2011. The alternating gray and white backgrounds represent the repetition of the 8-minute transmission format, which includes four distinct HF frequency combinations (between Beam 1 and Beam 2). Within each section, four distinct groups of data points ranging from ~105 to ~122 dB are clearly discernible, and these groups correspond to observations as a function of HF frequency combination. The data points ranging from ~80 to ~92 dB are performed during transmitter off times, and the largest of these amplitudes is used to estimate the noise floor.

[11] Figure 5 (top) provides an expanded-time view of the 90-second transmission period for Beam 1 at 5.8 MHz and Beam 2 at 4.5 MHz. During this 90-second period, Beam 1 continuously modulated the conductivity of the lower ionosphere, changing the modulation waveform every 18 seconds. At the same time, Beam 2 broadcast a CW wave every other second (alternating between on and off) increasing the power of the transmission in 1-dB steps over the course of 18 seconds. The observations shown in Figure 5 demonstrate that the first harmonic magnitude during CW-OFF periods is clearly stable over each 18-second period, varying by less than 1 dB. The CW-OFF signal stability indicates that the ionosphere and the strength of the auroral electrojet were stable over the transmission sequence. The first harmonic magnitude also clearly depends on the modulation waveform employed, as can be seen by the several-dB changes in

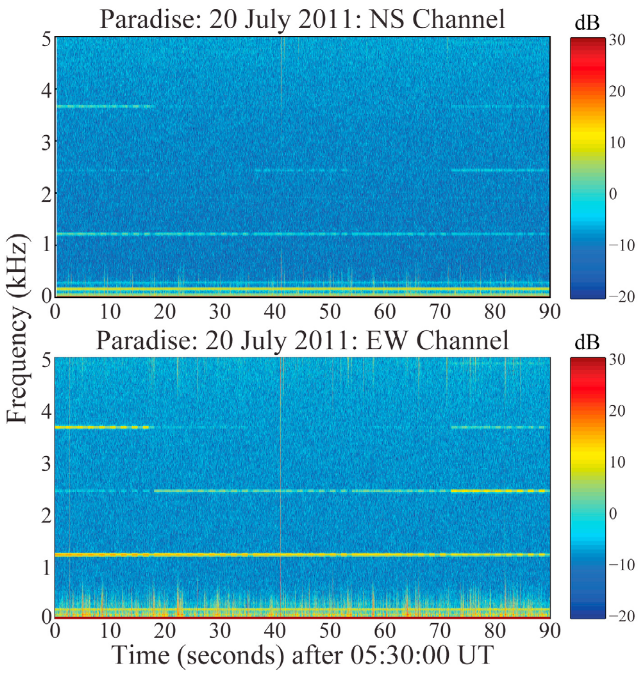

Figure 4. 90-second spectrograms of ELF observations at Paradise. Strong ELF waves are generated at 1225 Hz, as well as at higher-order harmonics.

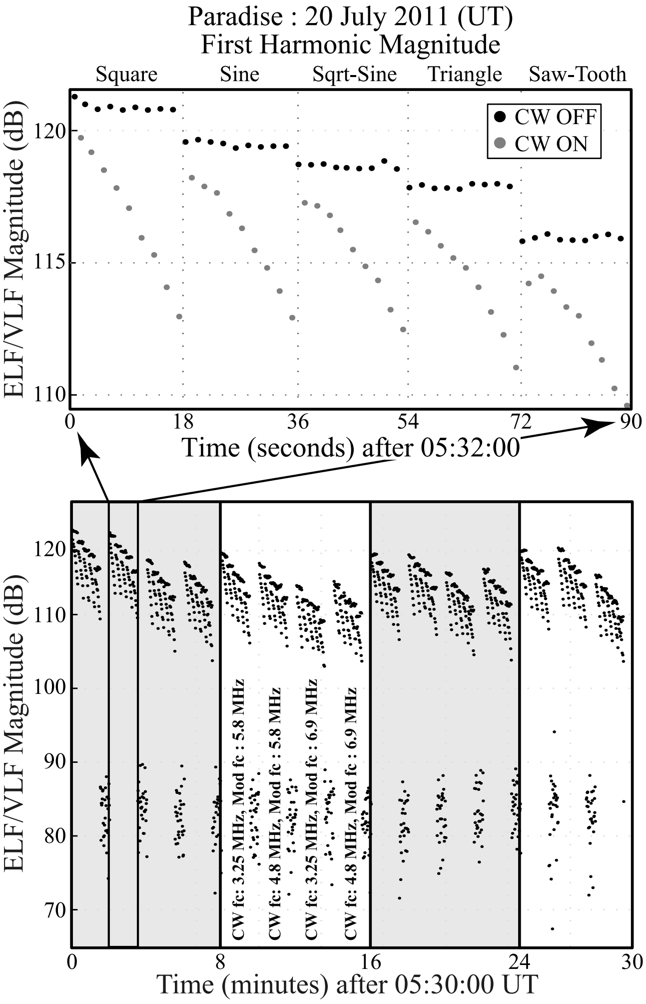

Figure 5. (top) 1225 Hz signal magnitudes over a 90-second transmission period. (bottom) 1225 Hz signal magnitude for the 30 minute transmission of 20 July 2011.

magnitude when the modulation waveform changes. These changes in magnitude are approximately consistent with Fourier analysis of the power envelope of the transmitted modulation waveform, as described by *Barr and Stubbe* [1993], and the slight deviations from Fourier analysis will be discussed in Section 4. During the CW-ON periods, the 1225 Hz signal magnitude is observed to decrease with increasing CW power for all modulation waveforms, consistent with the observations presented by *Moore and Agrawal* [2011].

[12] The data shown in Figures 3–5 are generally representative of our observations at all receiver sites and for all transmission periods, although the SNR varies with both time and site location. Table 1 summarizes the SNR observed at each receiver site for all days of observations during the transmission blocks. N/A entries indicate that the ELF receiver at Oasis had not yet been deployed to the site. To calculate the SNR levels shown in Table 1, the noise floor is approximated during periods when the HF transmitter is off.

[13] In the following section, we provide detailed analysis of these observations as a function of CW power, HF frequency combination, modulation waveform, and receiver location, and we compare the observations with the results of a dual-beam ionospheric HF heating model.

Table 1. The 1225 Hz SNR at Each Site for Each Day

Date (July 2011)	Time (UT)	SNR (dB) PD	OA	SC
0.8 20	0530	13–30	N/A	10–20
21	0730	0	N/A	0
0.8 25	0730	5–30	5–20	0–20

4. Analysis

[14] In this section, we compare observations and model predictions for the ELF signal magnitude received on the ground. The dual-beam ionospheric HF heating model used in this work is the same as that presented by *Moore and Agrawal* [2011], with its functionality extended to account for the five modulation waveforms employed in this work. The model simultaneously and self-consistently accounts for multibeam HF absorption and propagation through the *D*-region ionosphere. It takes as input parameters the directions of the HF beams, the HF frequencies and polarizations, the modulation frequency, and the ERPs of the beams. The ambient electron density and temperature profiles employed (see Figure 6) have been used in previous work [e.g., *Moore*

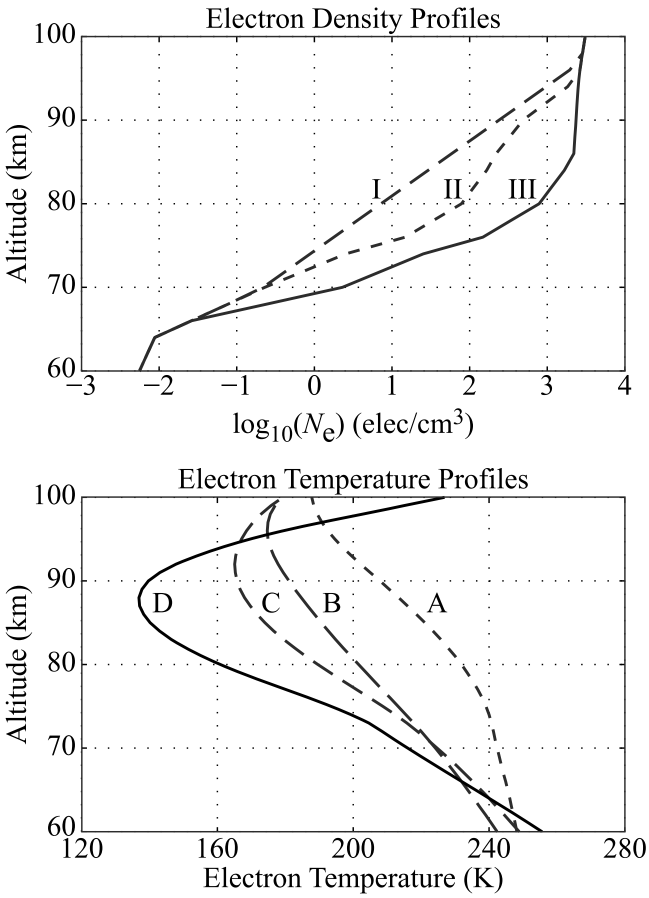

Figure 6. (top) Electron density and (bottom) electron temperature profiles used in this work.

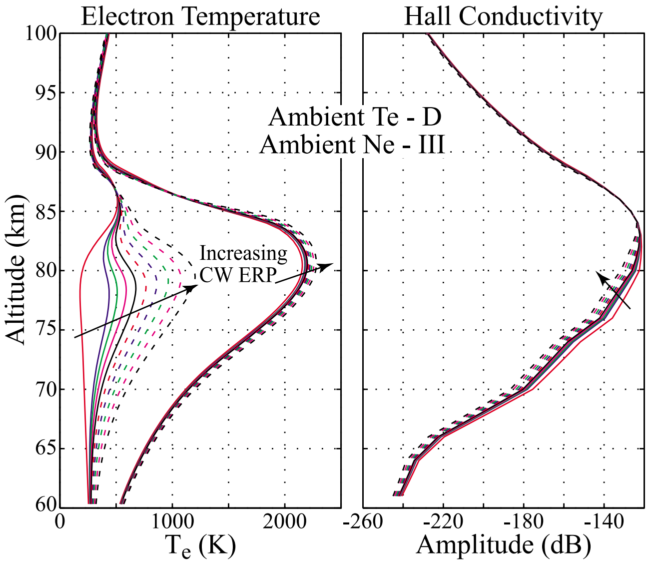

Figure 7. (left) Maximum and minimum electron temperatures achieved during the heating cycle for profile combination III-D as a function of CW ERP. (right) The corresponding amplitude of Hall conductivity modulation as a function of CW ERP.

and Agrawal, 2011]. The ambient electron temperature and neutral density profiles are provided by the MSISE-90 Atmosphere Model (http://ccmc.gsfc.nasa.gov/modelweb/) [*Labitzke et al.*, 1985; *Hedin*, 1991]. The dual-beam heating model calculates the complete time-evolution of the ionospheric conductivity components (Hall, Pedersen, and Parallel) as a function of time and space, and these conductivities are interpolated onto a 1-km^3 grid. The model thus inherently accounts for the group delays of the HF waves to each of the ionospheric grid points and for the temporal reaction of the plasma to the high-power HF signals. Both of these effects modify the phase of the ELF source currents as a function of space.

[15] Ionospheric ELF source currents are approximated by multiplying the Hall, Pedersen, and Parallel conductivities by the electrojet electric field strength, which is assumed to be constant throughout the *D*-region ionosphere and oriented parallel to the ground. Complication arises when one considers that *D*-region heating by the electrojet currents themselves may affect the amplitude of the radiated ELF fields. Model calculations (not shown) indicate that the conductivity modulation produced by modulated HF heating together with a 5 mV/m electrojet field strength is less than 0.2-dB different than that calculated with a 100 mV/m electrojet field, however. It is thus a good approximation to assume that the ELF source currents vary linearly with the electrojet field strength. Although this model assumes that the electron energy distribution remains Maxwellian throughout the heating process, the minimal impact of electrojet heating on the calculated conductivity modulation indicates that this assumption is likely to be valid even for fully kinetic models.

[16] With the distribution of ionospheric ELF source currents in hand, the magnetic field is calculated for a given ground-based receiver location assuming that the ELF source takes the form of spatially distributed set of dipoles over a ground plane [e.g., *Payne*, 2007]. For receiver locations within ~75 km of HAARP, this is a good approximation: *Payne* [2007] demonstrated that within ~75 km of HAARP the magnitude of the magnetic field calculated using a distributed dipole model closely matches that calculated using a more complete model that accounts Earth-ionosphere waveguide effects and for the secondary ionospheric currents generated during the modulated heating process. In order to mitigate the errors associated with neglecting these effects, the observations are normalized to the magnetic field observed during CW-OFF periods. This normalization cancels the effects of the Earth-ionosphere waveguide and the varying electrojet field strength to first order [*Barr and Stubbe*, 1993], allowing for the direct comparison of observations and modeling results.

[17] Because we present only normalized field values in this paper, it is worth noting that this model is fully capable of predicting absolute field strengths. For the profiles shown in Figure 6, and for reasonable (5–100 mV/m) values of the electrojet field strength [e.g., *Banks and Doupnik*, 1975; *Stubbe et al.*, 1981; *Papadopoulos et al.*, 2003; *Payne*, 2007], the magnetic field magnitudes predicted at a receiver located ~33 km from HAARP vary from ~40 fT to ~20 pT, which are very reasonable field values compared to past and present experimental observations [e.g., *Stubbe et al.*, 1982; *Rietveld et al.*, 1986, 1989; *Villaseñor et al.*, 1996; *Cohen et al.*, 2010]. The range of possible field values can be easily extended using a greater variety of ionospheric profiles. As mentioned above, however, absolute field measurements depend on Earth-ionosphere waveguide effects, on the generation of secondary ionospheric currents, and on the strength of the electrojet currents, in addition to the conductivity modulation produced by HF heating. In order to isolate the effects of HF heating, this paper exclusively presents normalized field observations.

[18] We now describe the dual-beam heating aspects of this ionospheric HF heating model. Figure 7 presents the results of an illustrative modeling example under dual-beam heating conditions. Figure 7 (left) shows the maximum and minimum electron temperatures achieved during a modulated heating cycle as a function of altitude. As the CW power increases, the minimum electron temperature increases to a greater extent than the maximum electron temperature, resulting in an overall reduction in electron temperature modulation. Figure 7 (right) shows the amplitude of Hall conductivity modulation as a function of altitude. Increased CW heating also results in the significant reduction of the Hall conductivity modulation at lower altitudes (below ~85 km). The reduction in conductivity modulation results in the overall reduction of magnetic field strength observed at the receiver.

[19] In the remainder of this section, we compare observations with the predictions of the dual-beam HF heating model as a function of CW HF power, CW HF frequency, modulated HF frequency, modulation waveform, and receiver location. Experimental observations are used to demonstrate that the change in conductivity modulation as a function of CW power is a measurable quantity that is sensitive to the ambient conditions of the *D*-region ionosphere. A theoretical analysis considering the cases of CW HF polarization and the modulation frequency of the modulated HF beam is also presented.

4.1. CW HF Power

[20] The four panels of Figure 8 show the observed (black traces) and predicted (color traces) ELF wave magnitudes as

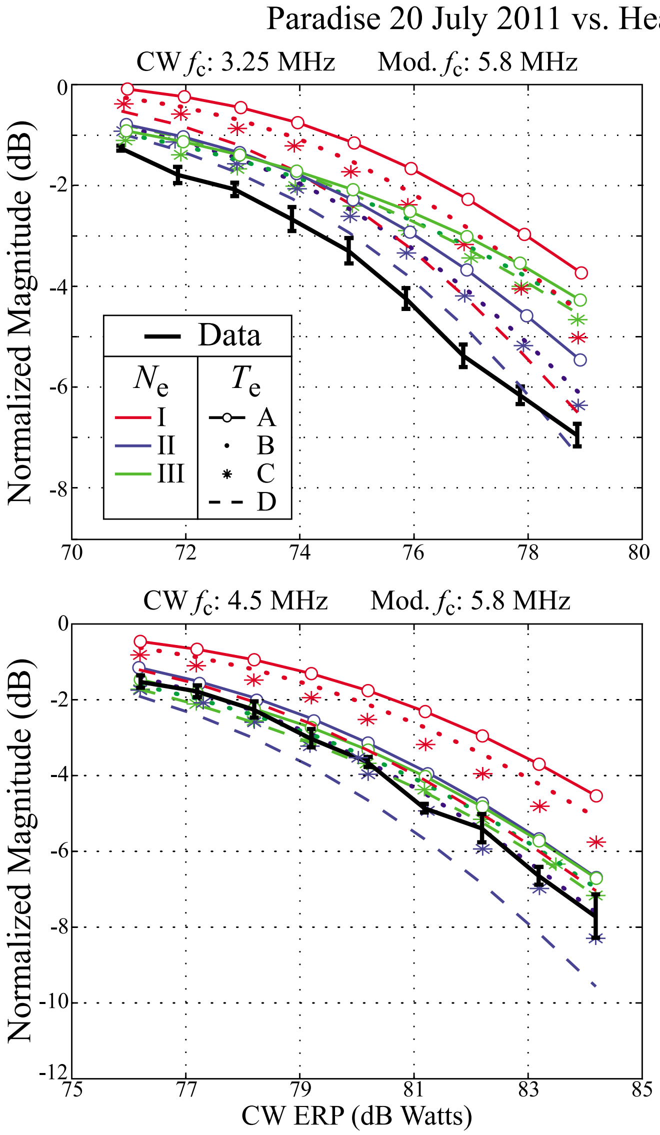

Figure 8. 1225 Hz signal magnitude observed at Paradise (solid black) together with dual-beam HF heating model predictions (color) for square-wave amplitude modulation. The four panels present results for four different Beam 1/Beam 2 HF frequency combinations and for twelve different N_e/T_e profile combinations.

a function of the effective radiated power (ERP) of the CW beam, with the four panels corresponding to the four Beam 1/Beam 2 HF frequency combinations employed. We point out that the scales of the four panels are different in order to clearly depict each of the traces within each panel. The predictions for all twelve combinations of electron density and electron temperature profiles are shown for each case, and each trace has been normalized so that 0 dB corresponds to the 1225 Hz magnitude observed during periods with the CW beam OFF. As mentioned previously, this normalization cancels the effects of the Earth-ionosphere waveguide to first order and provides a means to account for the variation in electrojet field strength over the course of the experiment [*Barr and Stubbe*, 1993].

[21] First considering only the experimental observations, all four traces exhibit similar variations with CW ERP: the normalized ELF magnitude decreases as a function of increasing CW ERP, and the rate of decrease increases with increasing CW ERP. Although we have only shown the first repetition of 20 July 2011 for each frequency combination on this figure, all other iterations of the experiment exhibit these same characteristic features. For all power levels with the CW beam ON, the normalized magnitudes at 1225 Hz are less than those observed during periods with the CW beam OFF, consistent with the observations reported by *Moore and Agrawal* [2011]. Comparing the left and right panels of Figure 8 (i.e., for constant CW HF frequency), subtle differences exist between the observations as a function of CW power, and we will consider these differences in detail in subsequent subsections. Comparing the top and bottom panels (i.e., for constant HF frequency of the modulated wave), it is evident that for a given ERP value, the 3.25 MHz CW signal suppresses

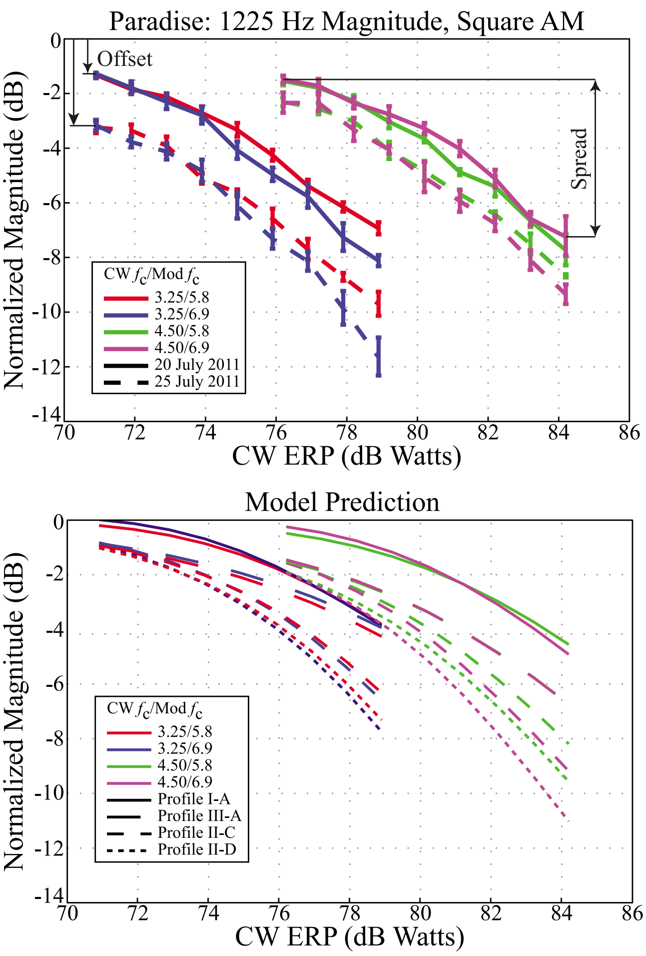

Figure 9. Normalized ELF magnitude as a function of CW ERP, highlighting the effects of Beam 1 (modulated) and Beam 2 (CW) HF frequency.

the ELF magnitude to a greater extent (~2 dB) than does the 4.5 MHz CW wave. We will consider this dependence in greater detail in Section 4.2.

[22] Now considering the model predictions together with the experimental observations, Figure 8 clearly demonstrates that all traces (both experimental and theoretical) exhibit a similar dependence on CW ERP: the normalized ELF magnitude decreases as a function of increasing CW ERP, and the rate of decrease increases with increasing CW ERP. In general, the predicted ELF magnitudes show good agreement with observations, although specific details of the traces clearly depend upon the specific ambient electron density and electron temperature profile employed. Nevertheless, comparing the left and right panels of Figure 8 (i.e., for constant CW HF frequency), the differences between model predictions as a function of Beam 1 frequency are very similar to those exhibited by the observations. Furthermore, comparing the top and bottom panels (i.e., for constant HF frequency of the modulated wave), the model predicts that the 3.25 MHz CW signal will suppress the ELF magnitude to a greater extent (~2 dB) than the 4.5 MHz CW wave for a constant ERP level, strikingly similar to observations.

[23] Having compared experimental observations with theoretical predictions as a function of CW power, we continue our analysis by comparing results as a function of the HF frequency of the CW beam.

4.2. CW HF Frequency

[24] Figure 9 (top) presents experimental observations of the 1225 Hz signal magnitude performed on 20 July 2011 (solid traces) and on 25 July (dashed traces) at Paradise (PD) as a function of CW ERP. The power steps for the two different CW frequencies employed span two distinct ERP ranges. In order to determine the dependence on CW frequency, we compare the 3.25/5.8 (red) traces with the 4.5/5.8 (green) traces and the 3.25/6.9 (blue) traces with the 4.5/6.9 (purple) traces. The observations performed on 20 July 2011 exhibit nearly identical dependencies on CW ERP (after discounting for the different CW frequency-dependent gains): the initial suppression offset and the spread of suppression as a function of CW power, as defined in the figure, are essentially the same. Observations performed on 25 July 2011, under different ambient ionospheric conditions, however, clearly indicate that the suppression offset is ~1–2 dB greater for 3.25 MHz than for 4.5 MHz and that the suppression spread as a function of CW ERP is ~1–2 dB greater for 3.25 MHz than for 4.5 MHz. In this case, the suppression offset and the spread are both different as a function of HF frequency combination. These experimental observations indicate that the received ELF magnitude as a function of CW frequency is sensitively dependent upon the ambient ionospheric conditions.

[25] Figure 9 (bottom) presents model predictions for four different ionospheric profile combinations (I-A, II-C, II-D, and III-A). The level of ELF magnitude suppression differs as a function of CW frequency, and this difference changes as a function of ionospheric profile combination, dependent upon both the ambient electron density and electron temperature profile employed. Modeling results exhibit both small and large differences in suppression offset and spread as a function CW frequency. We expect that a different set of ionospheric profiles will reproduce the large (~3-dB) initial suppression offset observed on 25 July 2011, although we have made no effort to do so here. Most importantly, both observations and model predictions indicate that the level of ELF magnitude suppression by additional CW heating sensitively depends on the frequency of the CW signal and on the ionospheric conditions.

[26] Having compared experimental observations with theoretical predictions as a function of CW HF frequency, we continue our analysis by comparing results as a function of the modulated HF frequency.

4.3. Beam 1 HF Frequency (Modulated)

[27] We continue to refer to Figure 9 to investigate the dependence on the modulated (Beam 1) HF frequency. In this case, we compare the 3.25/5.8 (red) traces with the 3.25/6.9 (blue) traces and the 4.5/5.8 (green) traces with the 4.5/6.9 (purple) traces. On a given day and for a given CW HF frequency, the normalized ELF magnitude for 5.8 MHz is extremely similar to that for 6.9 MHz. For both CW frequencies (3.25 and 4.5 MHz), the differences in ELF magnitude suppression are nearly negligible at low CW power levels. For a CW frequency of 3.25 MHz, at higher (>74 dBW ERP) CW power levels, the signals generated using 6.9 MHz are slightly more suppressed than those generated using

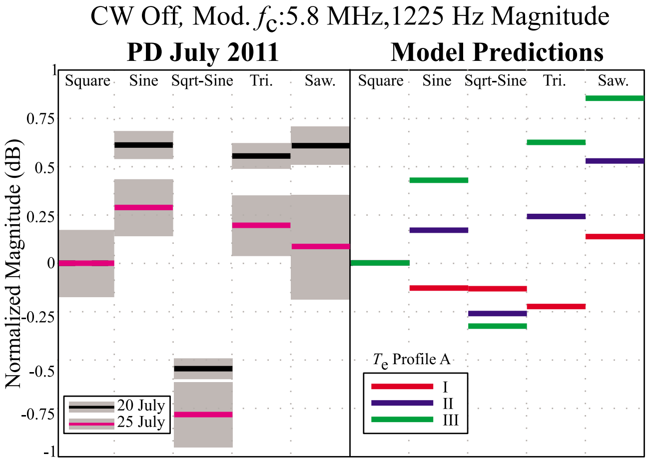

Figure 10. CW-OFF: ELF magnitude as a function of modulation waveform, normalized by the magnitude generated for square AM.

5.8 MHz, with the difference in suppression increasing with increasing CW power up to a maximum difference of 0.5–1.0 dB (depending on the day, and thereby ambient ionospheric conditions). For a CW frequency of 4.5 MHz, similar differences are observed at higher CW power levels (>80 dBW ERP), although the difference in the level of suppression is less than for the 3.25 MHz CW signal, maximizing at ~0.25 dB.

[28] The model predictions for the four different ambient ionospheric conditions shown in Figure 9 (bottom) exhibit the same general trends exhibited by the experimental observations: the difference in the level of suppression between Beam 1 frequencies increases with increasing CW power. For the ambient ionospheric combinations considered, the predictions indicate that ELF signals generated using 5.8 MHz may be more or less suppressed than those generated using 6.9 MHz. Additionally, 3.25 MHz may create larger or smaller differences than 4.5 MHz, depending on the ionospheric profile combination. At the highest CW power levels, the difference in suppression may be as high as 1.0 dB, also depending on the ambient ionospheric profile combination employed. Based on both experimental observations and theoretical predictions, we conclude that while the dependence on Beam 1 (modulated) HF frequency is measurable at these CW power levels, significant (~1-dB) differences are detectable only at higher CW power levels, when the ELF SNR is lower (and the error bars are higher). As a result, the difference in CW suppression as a function of Beam 1 frequency is a difficult measurement to perform in practice.

[29] Having compared experimental observations with theoretical predictions as a function of Beam 1 (modulated) HF frequency, we continue our analysis by comparing results as a function of amplitude modulation (AM) waveform.

4.4. Modulation Waveform

[30] Figure 10 (left) shows the normalized average ELF magnitude experimentally observed as a function of AM waveform on 20 July and 25 July 2011. These particular measurements were performed during CW-OFF periods, and they are normalized by the first Fourier harmonic component of the respective ideal signal waveforms, taking the average square-wave signal magnitude as a 0-dB reference. Accounting for the error bars, shown in gray, the difference in normalized signal magnitude measured between the two days varies between ~0.10 and ~0.80 dB as a function of modulation waveform, with the largest difference occurring for the saw-tooth waveform. We note that the 20 July 2011 observations are larger than the 25 July 2011 observations for all modulation waveforms. Because the transmission format did not change between the two days, these differences are attributable to the different ambient ionospheric conditions on the two days. The model predictions for the normalized ELF magnitude as a function of electron density (for electron temperature Profile A) are shown in Figure 10 (right). The model predictions exhibit variations as a function of ionospheric profile combination, with the largest (~0.80-dB) variations occurring for the triangle waveform. Comparing observations

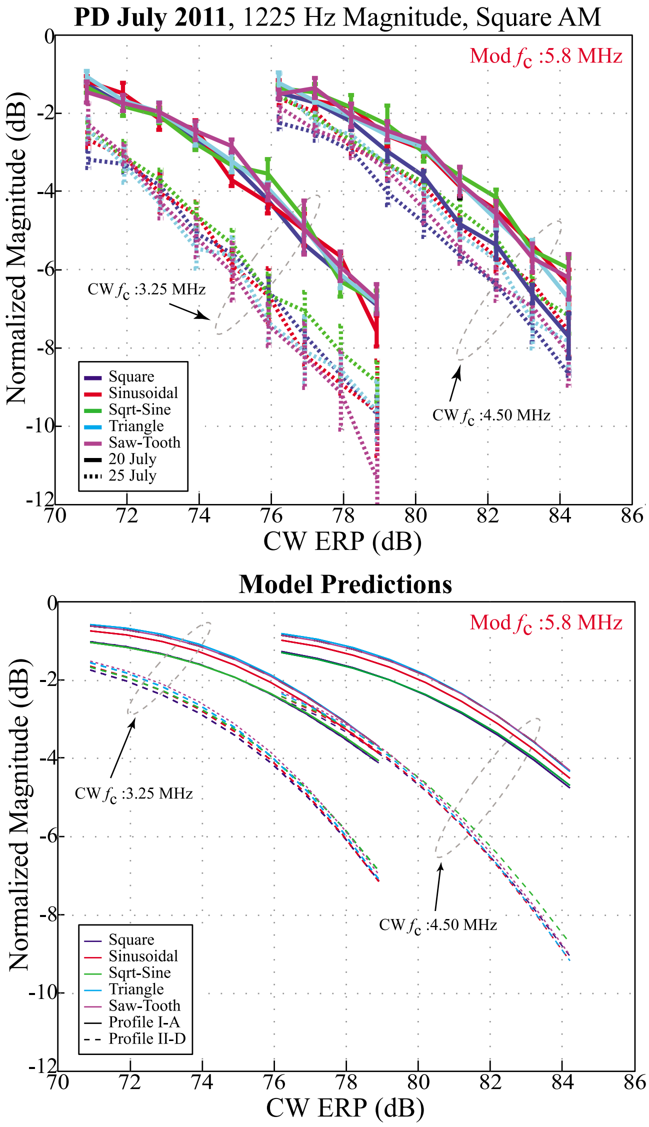

Figure 11. ELF magnitude as a function of CW ERP for five AM waveforms for CW f_c 3.25 MHz and modulated f_c 5.8 MHz for (top) experimental observations and (bottom) model predictions. Only very subtle variations in ELF magnitude are observed as a function of AM waveform.

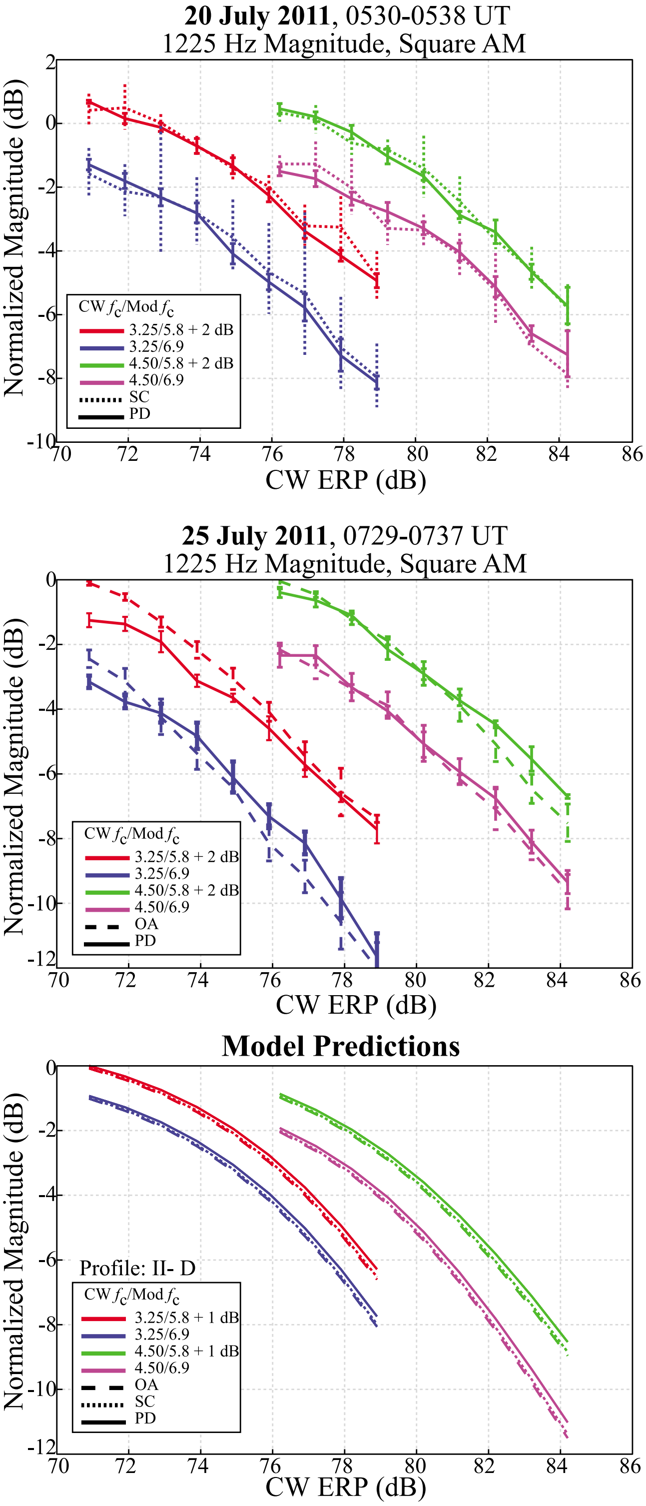

Figure 12. The normalized ELF magnitude as a function of ELF receiver location. Red and green traces have been offset vertically to facilitate visual comparison between the traces.

with the predictions of the theoretical model, all experimentally measured values are within ~0.5-dB of the theoretical results, with the worst correspondence occurring for the sqrt-sine modulation waveform. Considering that a CW beam is not required to perform this measurement, the SNR does not significantly suffer as a result (as opposed to the Beam 1 frequency case). It thus appears to be the case that careful observations of the relative magnitudes generated using different AM waveforms may yield independent information regarding the ambient ionospheric conditions.

[31] Now considering the effects of additional CW heating, Figure 11 (top) shows the normalized ELF magnitude at 1225 Hz as a function of CW power for a constant Beam 1 HF frequency of 5.8 MHz. The observations are presented for both 20 July (solid traces) and 25 July (dashed traces). On both days, the normalized ELF magnitude for all five AM waveforms produce nearly identical results at all CW ERP levels, with the singular exception of the square-wave modulation case for 5.8/4.5 MHz on 20 July. The results for a Beam 1 HF frequency of 6.9 MHz (not shown) are similar in all respects. Figure 11 (bottom) shows the model predictions for the five AM waveforms as a function of CW ERP, using two different sets of ambient ionospheric conditions (I-A and II-D). The predictions for both sets of ambient profiles exhibit extremely similar variations of ELF magnitude for all five modulation waveforms as a function of CW ERP, with the largest offsets (only ~0.25-dB) occurring for the triangle and saw-tooth waveforms. Based on these results, we conclude that additional CW power does not provide additional independent information about the ambient ionospheric conditions as a function of the modulation waveform. Considering the effects of CW heating on the higher-order harmonic content produced as a function of modulation waveform is beyond the scope of this paper.

[32] In the following section, we compare observations and model predictions for different ELF receiver locations as a function of CW power.

4.5. Receiver Location

[33] Figure 12 (top) shows the normalized ELF signal magnitude observed at Sinona Creek (SC, 33 km from HAARP) and at Paradise (PD, 98 km from HAARP) on 20 July 2011 as a function of CW ERP for the four combinations of HF frequencies employed. Note that two sets of traces in Figures 12 (top) and 12 (middle) have been falsely offset by 2 dB and two sets of model predictions (Figure 12, bottom) have been offset by 1 dB for aesthetic purposes in order to facilitate the comparison as a function of receiver location. The normalized ELF magnitudes observed at the two locations are essentially the same (within the error bars) for all CW power levels and all HF frequency combinations. The error bars for the Sinona Creek measurements are high (>2 dB in some cases), however. The deployment of an ELF receiver at Oasis (OA, 3 km from HAARP) enabled high SNR measurements at two receiver sites on 25 July 2011. Figure 12 (middle) shows the normalized ELF observations at Paradise and Oasis on 25 July. For the Beam 2 CW frequency of 4.5 MHz, the observations are very similar at the two sites and the error bars overlap at almost all CW power levels. The same is not true for the Beam 2 CW frequency of 3.25 MHz. At low (<76 dB) CW power levels, the ELF magnitude generated by 5.8 MHz observed at Paradise is lower than that observed at Oasis by ~1 dB. The difference decreases with increasing CW ERP. A similar variation is observed for the 6.9 MHz signal below 73 dB ERP, although the maximum difference is less than 0.25 dB. Figure 12 (bottom) shows the predicted normalized ELF magnitude

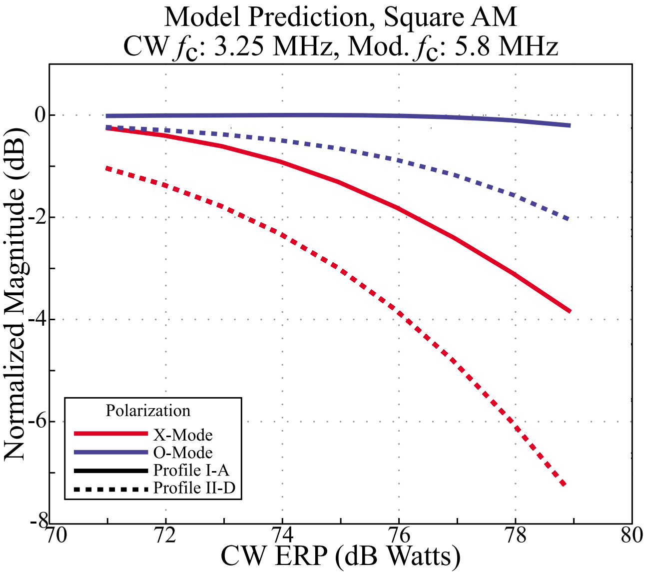

Figure 13. Theoretical predictions for normalized ELF magnitude as a function of CW HF beam polarization (X- versus O-mode).

as a function of CW ERP at all three ground based receivers. The model predictions are in general agreement with the observations, except at low power levels, and show that the normalized ELF magnitudes are expected to have comparable levels as a function of receiver location. We attribute the deviation observed at Paradise for low CW ERP levels to the effects of the Earth-ionosphere waveguide and possibly to the generation of secondary ionospheric currents [*Payne et al.*, 2007], neither of which are accounted for by our propagation model. Earth-ionosphere waveguide effects are expected to be important at receiver locations greater than ~75 km from HAARP [*Payne*, 2007], and Paradise is 98 km distant.

[34] It is interesting to note that at higher CW ERP levels and for higher CW HF frequencies, the observations presented in Figure 12 are very much in line with model predictions. We hypothesize that the altitude of the ELF source region plays a role in determining the relative importance of Earth-ionosphere waveguide effects at the receiver site. For instance, *Moore and Agrawal* [2011] showed (theoretically) that additional CW heating increases the altitude of the effective ELF source region. Furthermore, the ELF source produced by modulated heating at higher HF frequencies is expected to occur at somewhat higher altitudes than for lower HF frequencies [*Stubbe and Kopka*, 1977]. Last, higher altitude sources are expected to excite the Earth-ionosphere waveguide less effectively than lower altitude sources [e.g., *Tripathi et al.*, 1982]. Together, these considerations may explain the normalized ELF magnitudes observed at Paradise for low and high CW ERP levels.

[35] Based on the observations and theoretical modeling, we conclude that additional measurements at receiver locations within ~75 km of HAARP will not contribute a significant amount of additional information about the ambient *D*-region ionosphere. Nevertheless, additional observations at locations greater than ~100 km from HAARP could possibly provide more information regarding other effects, such as those related to the Earth-ionosphere waveguide or to secondary ionospheric currents.

[36] Having completed our comparison of experimental observations with model predictions, we now present theoretical predictions for the normalized ELF magnitude as a function of the polarization of the CW HF beam and the modulation frequency of the modulated beam.

4.6. Polarization

[37] It is well known that modulated X-mode heating produces higher amplitude ELF waves that does modulated O-mode heating [*Stubbe et al.*, 1981, 1982; *Ferraro et al.*, 1984; *James et al.*, 1984; *Villaseñor et al.*, 1996]. In order to increase the SNR of our observations, we choose to use an X-mode polarized HF beam to modulate the ionospheric conductivity for all experiments. In this section, we theoretically investigate the effects that are produced by changing the polarization of the CW beam, as opposed to that of the modulated HF beam. Figure 13 shows the model predictions for CW heating using both X- and O-mode polarizations for the CW beam. Results for two ionospheric profile combinations (I-A and II-D) are presented. In both cases, O-mode CW heating suppresses the normalized ELF magnitude to a lesser extent than X-mode heating. For Profile I-A, O-mode heating appears to have an almost negligible effect on the ELF magnitude, whereas for Profile II-D, O-mode heating produces 2 dB of suppression at the highest CW ERP level. Based on these model predictions, we suggest that the difference in the level of ELF magnitude suppression produced by X-mode and O-mode CW heating (1) is measurable, and (2) produces independent information regarding the ambient ionospheric conditions. For instance, for Profile I-A, the difference in the suppression produced by X- and O-mode CW heating increases with CW ERP from ~0.25 dB at the lowest CW ERP level to ~3.5 dB at the highest CW ERP level. For Profile II-D, the difference increases from ~0.75 dB to ~5.5 dB. Additionally, the suppression offsets and spreads are significantly different (>3 dB), especially at high CW power levels. Measurements comparing X- and O-mode CW suppression could significantly contribute to an analysis of ambient ionospheric conditions.

4.7. Modulation Frequency

[38] Figure 14 shows the predicted ELF magnitude as a function of CW ERP for two different modulation frequencies and for two different ambient ionospheric profile combinations. For both modulation frequencies, increasing the CW power increases the level of ELF magnitude suppression, and for both ionospheric profiles, the signal generated using the higher modulation frequency is suppressed to a lesser extent. The difference in suppression (as a function of modulation frequency) increases from ~0.25 dB at the lowest CW power level to 0.75–1.0 dB at the highest CW power level for both ionospheric profiles. While these differences as a function of CW power level are not as large as the differences produced by X- and O-mode heating, they are detectable. Nevertheless, the system response would need to be calibrated to a very tight tolerance at the different modulation frequencies to provide reliable observations as a function of modulation frequency. We thus conclude that while measurements comparing CW suppression as a

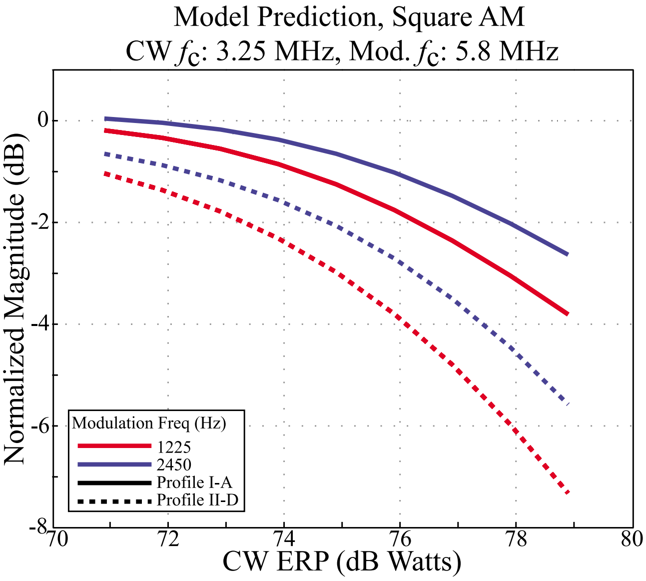

Figure 14. Theoretical predictions showing the normalized ELF magnitude for different modulation frequencies.

function of modulation frequency and CW power can provide additional information regarding the ambient ionospheric conditions, such measurements would be difficult to perform reliably in practice.

5. Discussion

[39] Experimental observations performed during power-stepped dual-beam ELF wave generation experiments at HAARP have been presented and compared to the predictions of a dual-beam ionospheric HF heating model. Comparisons were performed as a function of HF power, HF frequency, modulation waveform, and receiver location. Model predictions agree well with observations, demonstrating that the model incorporates the essential physics involved in multibeam HF heating of the lower ionosphere. We evaluated the sensitivity of the received ELF wave magnitude to these controllable parameters and interpreted the dependence on ambient ionospheric conditions. As a result, we have identified the types of transmissions that may provide a significant amount of information regarding the ambient conditions of the *D*-region ionosphere. While an inverse procedure to derive the ambient electron density and temperature profiles from these measurements remains to be presented, the observations and modeling presented herein strongly suggest that dual-beam ELF wave generation experiments can play an important role in a possible future *D*-region diagnostic.

[40] In many cases, the modeling results indicate that the suppression of ELF magnitude by additional CW heating depends sensitively on both the electron density and electron temperature profiles. In fact, one of the major difficulties in providing a *D*-region diagnostic for these parameters is simply to separate the effects of electron density and electron temperature. Figure 15 presents summary charts of ELF magnitude suppression as a function of CW ERP, with the traces organized by electron density profile. It is clear that for electron density Profiles 1 and 2, the electron temperature profile employed significantly impacts the resulting ELF signal magnitude. For electron density Profile 3, however, the results are essentially independent of electron temperature, indicating that for larger *D*-region electron densities, the effects of electron temperature are minimized.

[41] We conclude by enumerating our experimental and theoretical results:

[42] 1. For high CW power levels, the introduction of additional CW heating reduces the amplitude of the received ELF wave. The rate of ELF magnitude suppression increases with increasing CW power.

[43] 2. The level of ELF magnitude suppression depends on the CW frequency employed, and the level of suppression as a function of CW frequency is sensitively dependent on the ambient ionospheric conditions.

[44] 3. The level of ELF magnitude suppression also depends on the frequency of the modulated HF beam, although to a lesser extent than the CW frequency.

[45] 4. The ELF signal magnitude as a function of modulation waveform (without CW heating) also depends on the ambient ionospheric conditions, whereas the suppression supplied by additional CW heating is extremely similar as a function of modulation waveform.

[46] 5. ELF receivers located at significantly different distances from HAARP (3–98 km) register similar normalized ELF magnitudes at high CW power levels. Differences exist at lower CW power levels, and we attribute these differences to the effects of the Earth-ionosphere waveguide at larger distances.

[47] 6. A theoretical analysis predicts that O-mode CW heating may provide additional independent information to

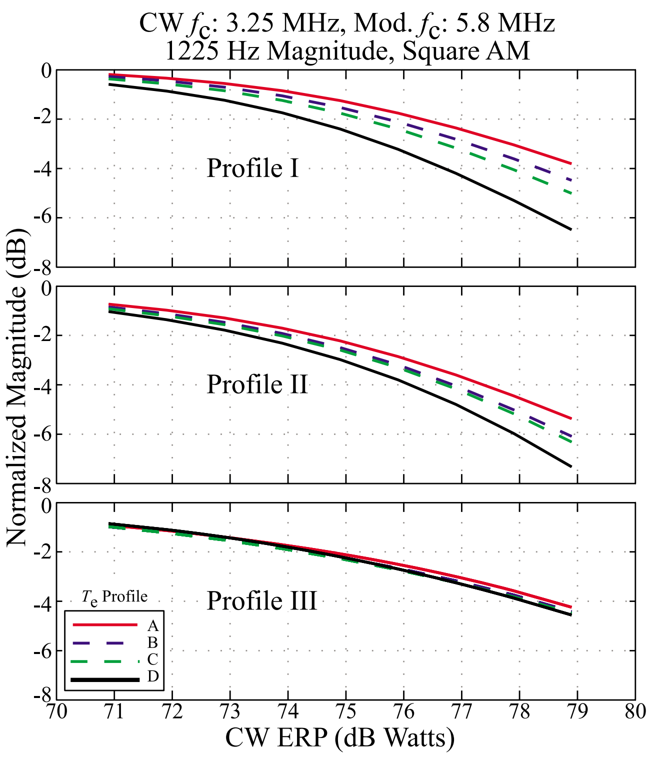

Figure 15. Model predictions for the normalized ELF magnitude as a function of electron density profile and electron temperature profile.

observations performed using X-mode CW heating and that these observations are sensitively dependent on the ambient conditions of the *D*-region.

[48] 7. Last, we predict that the effect of CW heating will decrease with increasing modulation frequency.

[49] **Acknowledgments.** This work is supported by DARPA grant HR0011-10-1-0061, DARPA contract HR0011-09-C-0099, NSF grants AGS-0940248 and ANT-0944639, and ONR grant #N000141010909 to the University of Florida.

[50] Robert Lysak thanks Joseph Payne and another reviewer for their assistance in evaluating this paper.

References

Banks, P. M., and J. R. Doupnik (1975), A review of auroral zone electrodynamics deduced from incoherent scatter radar observations, *J. Atmos. Terr. Phys.*, *37*, 951–972.

Barr, R., and P. Stubbe (1984a), ELF and VLF radiation from the "polar electrojet antenna", *Radio Sci.*, *19*, 1111–1122.

Barr, R., and P. Stubbe (1991a), ELF radiation from the Tromsø "Super Heater" facility, *Geophys. Res. Lett.*, *18*, 1035–1038.

Barr, R., and P. Stubbe (1991b), On the ELF generation efficiency of the Tromsø heater facility, *Geophys. Res. Lett.*, *18*, 1971–1974.

Barr, R., and P. Stubbe (1993), ELF harmonic radiation from the Tromsø heating facility, *Geophys. Res. Lett.*, *20*, 2243–2246.

Cohen, M. B., U. S. Inan, M. Golkowski, and M. J. McCarrick (2010), ELF/VLF wave generation via ionospheric HF heating: Experimental comparison of AM, beam painting, and geometric modulation, *J. Geophys. Res.*, *115*, A02302, doi:10.1029/2009JA014410.

Ferraro, A. J., H. S. Lee, R. Allshouse, K. Carroll, R. Lunnen, and T. Collins (1984), Characteristics of ionospheric ELF radiation generated by HF heating, *J. Atmos. Terr. Phys.*, *46*, 855–865.

Fujimaru, S., and R. C. Moore (2011), Analysis of time-of-arrival observations performed during ELF/VLF wave generation experiments at HAARP, *Radio Sci.*, *46*, RS0M03, doi:10.1029/2011RS004695.

Getmantsev, C. G., N. A. Zuikov, D. S. Kotik, L. F. Mironenko, N. A. Mityakov, V. O. Rapoport, Y. A. Sazonov, V. Y. Trakhtengerts, and V. Y. Eidman (1974), Combination frequencies in the interaction between high-power short-wave radiation and ionospheric plasma, *JETP Lett.*, *20*, 101–102.

Hedin, A. E. (1991), Extension of the MSIS thermospheric model into the middle and lower atmosphere, *J. Geophys. Res.*, *96*, 1159–1172.

James, H. G., R. L. Dowden, M. T. Rietveld, P. Stubbe, and H. Kopka (1984), Simultaneous observations of ELF waves from an artificially modulated auroral electrojet in space and on the ground, *J. Geophys. Res.*, *89*, 1655–1666.

Jin, G., M. Spasojevic, M. B. Cohen, U. S. Inan, and N. G. Lehtinen (2011), The relationship between geophysical conditions and ELF amplitude in modulated heating experiments at HAARP: Modeling and experimental results, *J. Geophys. Res.*, *116*, A07310, doi:10.1029/2011JA016664.

Labitzke, K., J. J. Barnett, and B. Edwards (Eds.) (1985), *Handbook MAP 16, SCOSTEP*, Univ. of Ill., Urbana.

Milikh, G. M., K. Papadopoulos, M. McMarrick, and J. Preston (1999), ELF emission generated by the HAARP HF-heater using varying frequency and polarization, *Izv. Vyssh. Uchebn. Zaved Radiofiz.*, *42*, 728–735.

Moore, R. C. (2007), ELF/VLF wave generation by modulated HF heating of the auroral electrojet, PhD thesis, Stanford Univ., Stanford, Calif.

Moore, R. C., and D. Agrawal (2011), ELF/VLF wave generation using simultaneous CW and modulated HF heating of the ionosphere, *J. Geophys. Res.*, *116*, A04217, doi:10.1029/2010JA015902.

Moore, R. C., U. S. Inan, and T. F. Bell (2006), Observations of amplitude saturation in ELF/VLF wave generation by modulated HF heating of the auroral electrojet, *Geophys. Res. Lett.*, *33*, L12106, doi:10.1029/2006GL025934.

Moore, R. C., U. S. Inan, T. F. Bell, and E. J. Kennedy (2007), ELF waves generated by modulated HF heating of the auroral electrojet and observed at a ground distance of 4400 km, *J. Geophys. Res.*, *112*, A05309, doi:10.1029/2006JA012063.

Papadopoulos, K., C. L. Chang, P. Vitello, and A. Drobot (1990), On the efficiency of ionospheric ELF generation, *Radio Sci.*, *25*, 1311–1320.

Papadopoulos, K., T. Wallace, M. McCarrick, G. M. Milikh, and X. Yang (2003), On the efficiency of ELF/VLF generation using HF heating of the auroral electrojet, *Plasma Phys. Rep.*, *29*, 561–565.

Payne, J. A. (2007), Spatial structure of very low frequency modulated ionospheric currents, PhD thesis, Stanford Univ., Stanford, Calif.

Payne, J. A., U. S. Inan, F. R. Foust, T. W. Chevalier, and T. F. Bell (2007), HF modulated ionospheric currents, *Geophys. Res. Lett.*, *34*, L23101, doi:10.1029/2007GL031724.

Rietveld, M. T., and P. Stubbe (1987), Ionospheric demodulation of powerful pulsed radio waves: A potential new diagnostic for radars suggested by Tromsø heater results, *Radio Sci.*, *22*, 1084–1090.

Rietveld, M. T., H. Kopka, E. Nielsen, P. Stubbe, and R. L. Dowden (1983), Ionospheric electric field pulsations: A comparison between VLF results from an ionspheric heating experiment and STARE, *J. Geophys. Res.*, *88*, 2140–2146.

Rietveld, M. T., H. Kopka, and P. Stubbe (1986), *D*-region characteristics deduced from pulsed ionospheric heating under auroral electrojet conditions, *J. Atmos. Terr. Phys.*, *48*(4), 311–326.

Rietveld, M. T., P. Stubbe, and H. Kopka (1989), On the frequency dependence of ELF/VLF waves produced by modulated ionospheric heating, *Radio Sci.*, *24*(3), 270–278, doi:10.1029/RS024i003p00270.

Stubbe, P., and H. Kopka (1977), Modulation of the polar electrojet by powerful HF waves, *J. Geophys. Res.*, *82*(16), 2319–2325, doi:10.1029/JA082i016p02319.

Stubbe, P., H. Kopka, and R. L. Dowden (1981), Generation of ELF and VLF waves by polar electrojet modulation: Experimental results, *J. Geophys. Res.*, *86*, 9073–9078.

Stubbe, P., H. Kopka, M. T. Rietveld, and R. L. Dowden (1982), ELF and VLF generation by modulated HF heating of the current carrying lower ionosphere, *J. Atmos. Terr. Phys.*, *44*, 1123–1135.

Tomko, A. A., A. J. Ferraro, and H. S. Lee (1980), *D* region absorption effects during high-power radio wave heating, *Radio Sci.*, *15*(3), 675–682.

Tripathi, V. K., C. L. Chang, and K. Papadopoulos (1982), Excitation of the earth-ionosphere waveguide by an ELF source in the ionosphere, *Radio Sci.*, *17*, 1321–1326.

Villaseñor, J., A. Y. Wong, B. Song, J. Pau, M. McCarrick, and D. Sentman (1996), Comparison of ELF/VLF generation modes in the ionosphere by the HIPAS heater array, *Radio Sci.*, *31*, 211–226.